

Behavior of the current in the asymmetric quantum multibaker map

Leonardo Ermann,^{1,2} Gabriel G. Carlo,¹ and Marcos Saraceno^{1,3}

¹*Departamento de Física, CNEA, Libertador 8250, (C1429BNP) Buenos Aires, Argentina*

²*Departamento de Física, FCEyN, UBA, Pabellón 1 Ciudad Universitaria, C1428EGA Buenos Aires, Argentina*

³*Escuela de Ciencia y Tecnología, UNSAM, Alem 3901, B1653HIM Villa Ballester, Argentina*

(Dated: October 24, 2018)

Recently, a new mechanism leading to purely quantum directed transport in the asymmetric multibaker map has been presented. Here, we show a comprehensive characterization of the finite asymptotic current behavior with respect to the \hbar value, the shape of the initial conditions, and the features of the spectrum. We have considered different degrees of asymmetry in these studies and we have also analyzed the classical and quantum phase space distributions for short times in order to understand the mechanisms behind the generation of the directed current.

PACS numbers: 05.45.Mt, 05.40.Jc, 05.60.-k

I. INTRODUCTION

There is a great interest in the study of directed transport in unbiased periodic systems. This phenomenon, also referred to as the ratchet effect, was initially considered by Feynman [1]. It can be classically ascribed to breaking all spatiotemporal symmetries leading to momentum inversion [2]. This allows a net current generation. For example, in non-Hamiltonian systems chaotic attractors need to be asymmetric [3] whereas in Hamiltonian ones (with mixed phase spaces) a chaotic layer should have this property [4]. Many times the same principle translates almost directly into the quantum domain [5], but in other cases more complex behaviors arise [6].

Since the first studies the relevance of this subject has been steadily growing, and several fundamental questions about the origin and properties of the net current have been answered [7]. However, the considerable amount of possible applications have opened a very broad field of research. In fact, a great and increasing number of experiments implement different kinds of ratchets. In biology, molecular motors principles can be understood on these grounds [8]. Also, they can be useful to develop nanodevices like rectifiers, pumps, particle separators, molecular switches and transistors [9]. Cold atoms and Bose-Einstein condensates have emerged as a very active area of application of these ideas, and the first experiments have initiated an activity that continues until present [10]. These efforts have led to the very recent success in transporting Bose-Einstein condensates for particular initial conditions by relying on purely quantum ratchet accelerators mechanisms [11]. Such experiments involve essentially the atom optics kicked rotor [12] at quantum resonance. In this system the current has no classical analogue and can be generated by just breaking the spatial symmetry [13]. Though the experimental realization of some proposed models is still demanding and the theoretical explanations are still not complete, ongoing studies show several new proposals [14]. They include ways of coherently controlling the ballistic energy growth of the atoms [15].

In order to investigate the mechanisms leading to net transport generation in quantum systems we have recently introduced an asymmetric version of the quantum multibaker map that shows a finite asymptotic current with no classical counterpart [16]. This is a paradigmatic model in classical and quantum chaos, but also in statistical mechanics [17, 18]. In this work we study the properties of the directed current in depth. We provide with a characterization of its behavior as a function of the \hbar value, the initial conditions and the spectrum features. All this has been considered for different values of the main parameter which determines the degree of spatial asymmetry. With this results at hand we proceed further to study the classical and quantum versions of the phase space distributions for short times. This shows the way in which the quantum current arises and the classical one does not, providing with a firm ground in order to understand the mechanisms involved. We finally make a comparison with the behavior of the system for longer evolutions of the order of the Heisenberg time.

In the following we describe the organization of this paper. In Section II we present our model in detail and the methods we have used to study it. We have chosen to divide this Section in four parts. Firstly, we formulate the classical and quantum propagators, then we explain some properties of the second one that are useful for the time evolution. Also, we introduce an asymptotic expression for the coarse-grained current, which is the main quantity under investigation. Finally the symmetry properties are explained. In Section III we analyze the current behavior as a function of \hbar , the initial conditions, and the spectrum shape. In Section IV we show the connection between the symmetries and the current generation by focusing on the classical and quantum phase space distributions for short times. We establish how the degree of asymmetry influences the features of the system studied in the previous Section. Finally, Section V is devoted to the conclusions.

II. MODEL AND METHODS

A. Classical and quantum propagators

The classical multibaker map [17] is defined in a phase space consisting of a lattice of unit square cells in position direction and confined in momentum ($p \in [0, 1)$). A phase space point can be completely defined by the number x ($x \in \mathbb{Z}$) of the cell to which it belongs and the position and momentum inside of it ($q, p \in [0, 1)$). The action of the map is a composition of an internal evolution inside of each cell (the baker map), followed by a translation along the lattice given by

$$M_s = T \circ B_s. \quad (1)$$

In this expression B_s is the asymmetric baker's map in the unit square phase space cell x . This is the area preserving map

$$B_s(q, p) \equiv \begin{cases} (\frac{1}{s}q, sp) & 0 \leq q < s \\ ((1-s)^{-1}(q-s), (1-s)p+s) & s \leq q < 1 \end{cases} \quad (2)$$

It can be clearly seen that the degree of asymmetry is controlled by the parameter s , and that there are two different Lyapunov exponents $\lambda_1 = -\ln(s)$, $\lambda_2 = -\ln(1-s)$. On the other hand T corresponds to an unbiased translation along the lattice, defined by

$$T = \begin{cases} (x+1, q, p) & 0 \leq q < 1/2 \\ (x-1, q, p) & 1/2 \leq q < 1 \end{cases} \quad (3)$$

This translation can only occur among adjacent cells and depends on the position inside of them. The geometric action of the asymmetric multibaker map (AMBM) can be seen in Fig. 1. The asymmetric quantum multibaker map (AQMBM) is defined in a Hilbert space \mathcal{H} which is the direct product of the lattice space (\mathcal{H}_L), and the individual cell space (\mathcal{H}_B), $\mathcal{H} = \mathcal{H}_L \otimes \mathcal{H}_B$ [18, 19]. In this work we will consider even D -dimensional internal subspaces \mathcal{H}_B on a torus (where $h = 1/D$), and infinite dimensional lattice subspaces. The translation over the lattice will be similar to the classical one. The dependence on the position inside of each cell is now given by the unbiased projectors \hat{P}_R and \hat{P}_L . These operators perform the projection on the right and left half of the position basis inside of each cell, satisfying $\hat{P}_R + \hat{P}_L = \hat{I}$ and $\text{Tr}(\hat{P}_R) = \text{Tr}(\hat{P}_L) = D/2$. Therefore, the AQMBM can be written as

$$\hat{M}_s \equiv \hat{T} \circ \hat{B}_s = \left(\hat{U} \otimes \hat{P}_R + \hat{U}^\dagger \otimes \hat{P}_L \right) \left(\hat{I} \otimes \hat{B}_s \right) \quad (4)$$

where \hat{U} is a unitary translation operator acting on the lattice subspace $\hat{U}|x\rangle = |x+1\rangle$ (with $\{|x\rangle, x = \dots, -2, -1, 0, 1, 2, \dots\}$ taken as the position basis set of the lattice). \hat{B}_s is

$$\hat{B}_s = \hat{G}_D^\dagger \begin{pmatrix} \hat{G}_{D_1} & 0 \\ 0 & \hat{G}_{D_2} \end{pmatrix} \quad (5)$$

$$\left(\hat{G}_D \right)_{kl} \equiv D^{-1/2} e^{-i2\pi(k+1/2)(l+1/2)/D}. \quad (6)$$

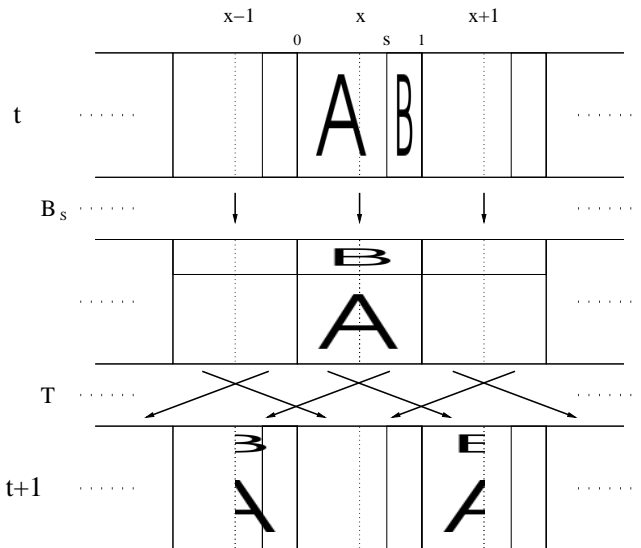


Figure 1: Geometric action of the asymmetric multibaker map. One iteration of the map corresponds to a composition of an internal evolution (given by the asymmetric baker map), and a translation among adjacent cells (which depends on the position inside of them).

This is the asymmetric quantum baker's map with antiperiodic boundary conditions, i.e., the corresponding generalization of the quantum symmetric one [20, 21]. In this case only the values of s such that $D_1 = sD$ and $D_2 = D - D_1$ are positive integer numbers are allowed.

B. Time evolution

The time evolution of an initial state can be computed straightforwardly in both classical and quantum cases in terms of the propagators given in Eq. (1) and Eq. (4), respectively. As usually happens in directed transport studies we are interested in the behavior of an initially localized distribution of particles. For that reason, we will focus on initial states which are located in a single site of the lattice. In the classical case the initial state will be a uniform probability distribution with the shape of a momentum band of width δp and extending completely along the q coordinate of the initial cell.

Correspondingly, in the quantum case we will always start with separable initial states of the form $\rho_0 = \rho_0^L \otimes \rho_0^B$. In this case, ρ_0^L is the initial state in the lattice space, in practice a given position basis element. On the other hand, ρ_0^B is a mixed superposition of Δp momentum eigenstates of the individual cell subspace. This kind of initial state is the quantum analogue of the previously described classical one, therefore we will take $\Delta p = D\delta p$ to make both of them fully comparable.

The quantum state at time t , $\rho(t)$, is the result of the

discrete time propagation of the initial state given by

$$\rho(t) = \left(\hat{M}_s\right)^t \rho_0 \left(\hat{M}_s^\dagger\right)^t. \quad (7)$$

This expression can be simplified noting that in \hat{M}_s the translation operator \hat{U} becomes diagonal in the momentum basis of the lattice subspace $\{|k\rangle\}$

$$\hat{U}|k\rangle = e^{-ik}|k\rangle \quad (8)$$

where by the previous definition

$$|k\rangle = \sum_{x=-\infty}^{\infty} |x\rangle e^{ikx}. \quad (9)$$

Thanks to this property we can better handle the action of the AQMBM of Eq. (4) on a given state of our system. If we define $\hat{B}_{s,k}$ as an operator acting on individual cell states $|\Psi_B\rangle$ and being parametrized by the lattice momentum value k , \hat{M}_s can be rewritten as

$$\hat{M}_s (|k\rangle \otimes |\Psi_B\rangle) = |k\rangle \otimes \hat{B}_{s,k} |\Psi_B\rangle, \quad (10)$$

where by definition

$$\hat{B}_{s,k} \equiv \begin{pmatrix} e^{-ik} & 0 \\ 0 & e^{ik} \end{pmatrix} \hat{B}_s \quad (11)$$

Then, the quantum asymptotic time evolution turns into the study of the eigenvalues and eigenvectors of this last operator, as we will see in the following.

C. Coarse-grained current

For a given ensemble of classical initial conditions, we define $p_{class}(x, t)$ as the probability of the particle to be in the x lattice cell at time t . In this way we can compute the mean value of the coarse-grained position as $\langle x \rangle = \sum_x x p_{class}(x, t)$ (which is the average value of the cell position x). Then, the coarse-grained current is calculated as the difference between this mean value at time t and the same value taken at an earlier time $t - 1$. The current $J_{class} = \langle x(t) \rangle - \langle x(t-1) \rangle$ can be derived from the first moment of the classical distribution, but higher moments can be calculated also in this way, i.e. disregarding the fluctuations that take place inside each cell.

For the quantum evaluation we first consider the probability distribution of the particle to be in the x lattice cell after t iterations of the map. This is given by

$$p(x, t) = \text{Tr} [\rho(t) (|x\rangle\langle x| \otimes I)] \quad (12)$$

In particular, for an initial state localized in one site (i.e., for which we take $\rho_0^I = |0\rangle\langle 0|$) and in the lattice momentum representation, the previous expression becomes

$$p(x, t) = \int \int \frac{dkdk'}{(2\pi)^2} e^{-ix(k-k')} \text{Tr} \left[\left(\hat{B}_{s,k'} \right)^t \rho_0^B \left(\hat{B}_{s,k}^\dagger \right)^t \right] \quad (13)$$

The coarse grained position is obtained by tracing out each cell's internal degrees of freedom (q). The moments of this quantity can now be easily calculated using the probability distribution $p(x, t)$

$$\langle x^m \rangle_t = \sum_x x^m p(x, t). \quad (14)$$

Finally, in complete analogy to the classical definition we will take the quantum coarse-grained current to be

$$J(t) = \langle x \rangle_t - \langle x \rangle_{t-1}. \quad (15)$$

Following closely Brun *et al.* [22], we insert the identity

$$\frac{1}{2\pi} \sum_x x^m e^{-ix(k-k')} = i^m \delta^{(m)}(k - k') \quad (16)$$

into Eq. (14), and integrating by parts we obtain

$$\langle x^m \rangle_t = \frac{i^m}{2\pi} \int dk \text{Tr} \left[\rho_0^B \left(\hat{B}_{s,k}^\dagger \right)^t \frac{d^m}{dk^m} \left(\hat{B}_{s,k} \right)^t \right]. \quad (17)$$

Therefore the first moment can be written as

$$\langle \hat{x} \rangle_t = \frac{i}{2\pi} \int dk \text{Tr} \left[\rho_0^B \left(\hat{B}_{s,k}^\dagger \right)^t \left(\frac{d}{dk} \left(\hat{B}_{s,k} \right)^t \right) \right], \quad (18)$$

where

$$\begin{aligned} \frac{d\hat{B}_{s,k}}{dk} &= \left(-ie^{-ik} \hat{P}_R + ie^{ik} \hat{P}_L \right) \hat{B}_s = -i\hat{Z} \hat{B}_{s,k}, \text{ and} \\ \hat{Z} &\equiv \hat{P}_R - \hat{P}_L. \end{aligned} \quad (19)$$

Substituting this into Eq. (18), the coarse-grained position mean value becomes

$$\langle \hat{x} \rangle_t = \sum_{j=1}^t \int \frac{dk}{2\pi} \text{Tr} \left[\rho_0^B \left(\hat{B}_{s,k}^\dagger \right)^j \hat{Z} \left(\hat{B}_{s,k} \right)^j \right]. \quad (20)$$

A similar procedure could be followed to obtain higher moments.

The time dependence in Eq. (20) can be made explicit by considering the spectral properties of the map $\hat{B}_{s,k}$

$$\hat{B}_{s,k} |\phi_l(k)\rangle = \exp(i\theta_l(k)) |\phi_l(k)\rangle. \quad (21)$$

In this basis the initial cell distribution is

$$\rho_0^B = \sum_{l,l'} a_{ll'}(k) |\phi_l(k)\rangle \langle \phi_{l'}(k)|. \quad (22)$$

Substituting this into Eq. (20) for the first moment we obtain

$$\langle x \rangle_t = \int \frac{dk}{\pi} \sum_{l,l'} a_{ll'}(k) \langle \phi_l(k) | \hat{Z} | \phi_{l'}(k) \rangle \sum_{j=1}^t e^{i(\theta_{l'}(k) - \theta_l(k))j}. \quad (23)$$

No approximations have been made in this derivation. If the spectrum has no degeneracies, as will be the case

for chaotic maps most of the terms in Eq. (23) will be highly oscillatory; hence, over time, they will average to zero. Only the diagonal terms in the above sum are nonoscillatory, allowing us to write

$$\langle x \rangle_t = J_\infty t + \text{oscillatory terms}, \quad (24)$$

where

$$J_\infty = \int \frac{dk}{2\pi} \sum_l a_{ll}(k) Z_{ll}(k) \quad (25)$$

$$Z_{ll}(k) \equiv \langle \phi_l(k) | \hat{Z} | \phi_l(k) \rangle. \quad (26)$$

In these expressions, J_∞ is the asymptotic value of the coarse-grained current defined in Eq. (15). The quantity $a_{ll}(k)$ corresponds to the projection of the initial state in the basis of eigenstates as previously stated, and $Z_{ll}(k)$ is a kind of right-left balance of each eigenstate.

This completes the description of the methods used to study our system. In the following we will explain some symmetry considerations relevant for the directed transport mechanism.

D. Symmetry properties

By looking at Fig. 1 the first thing that can be seen is that, though the baker map we consider is asymmetric, the transport term is unbiased. The transport is only due to this translation, that maps the same volume of phase space to the right and left. Quantum mechanically this also means that there is no tunneling effects from cell to cell. It has been shown that the presence of the net classical transport is originated from breaking all spatiotemporal symmetries that leave the system unchanged but change the sign of the (coarse-grained) current [2]. There are two transformations that fulfill these conditions, let us consider first

$$S_I : q \rightarrow 1 - q; p \rightarrow 1 - p,$$

acting on each cell, and leaving the transport term T unchanged. Under the action of S_I , the q and p coordinates are reflected with respect to their midpoints at each cell, and the map B_s transforms to B_{1-s} (we underline that this is valid in the classical and in the quantum case). For $s = 1/2$, i.e. the symmetrical Baker map, this transformation is a symmetry of the system. But it also changes the sign of the coarse-grained current, since a given trajectory that is transported to the left (right) at each iteration is now transported to the right (left). For other values of s the symmetry is broken. The other transformation is

$$S_{II} : q \rightarrow p; p \rightarrow q; T \rightarrow T^{-1}; t \rightarrow -t,$$

where the q and p part acts on each cell. This is the time reversal symmetry, present for any value of s . This transformation leaves the system unchanged, but reverses

all trajectories and consequently changes the sign of the coarse-grained current. This forbids any classical current for unbiased initial conditions. In previous studies we have found transient effects for biased conditions but they disappear very rapidly due to the exponential mixing property of the Baker map.

Finally we will refer to the symmetry properties of the coarse-grained current. J is an odd function of s around $s = 0.5$, i.e. $\langle J_s \rangle = -\langle J_{1-s} \rangle$. In fact, if we apply the symmetry transformation S_I to Eq. (7), and then trace out the internal degrees of freedom inside of each cell we obtain that $p_s(x, t) = p_{1-s}(-x, t)$ for all t . This result is valid for any initial ρ_0^B symmetrical under S_I .

III. QUANTUM CURRENT BEHAVIOR

In this Section we analyze the most important aspects of the quantum directed current, providing with a comprehensive understanding of its behavior. In the first place, we study the transition towards the classical limit that allows us to see the way in which the net transport vanishes. For that purpose we have numerically evaluated the asymptotic value of the coarse-grained quantum current J_∞ by means of Eq. (25). This has been done for all possible values of the quantum asymmetry parameter $s = D_1/D$, taking only $s \geq 0.5$ thanks to the symmetry property explained in the Section II. In order to have the same classical limit for all the $h = 1/D$ values, we have taken as initial conditions equal probability mixtures of an (integer) number $\Delta p = D/10$ of central momentum eigenstates. The results can be seen in Fig. 2, where the solid line corresponds to a dimension $D = 300$ for the Hilbert space of the cell, and the dots correspond to all possible values of D which are divisible by 10, between $D = 20$ and $D = 290$.

We can see that the currents corresponding to $D_1 = D - 1$ and $D_1 = D - 2$ are clearly different from the general behavior, we will come back to this particular feature later on when we analyze the spectrum. However, we note that there is a global convergence to the solid line, though the dependence on s is rather non-trivial. In fact, the current behavior (with the exception of the last points for $D_1 = D - 1$ and $D_1 = D - 2$) can be divided into two parts. The first one corresponds to $s \lesssim 0.7$, where J_∞ is already small for the maximum D we have taken in our calculations. In this respect, the current seems to vanish much faster than in the $s \gtrsim 0.7$ domain, in which higher values can be observed. It seems that the quantum effects are enhanced if one of the two parts in which the phase space is divided is clearly smaller than the other. We have found a similar effect in our studies of the current dependence on the initial conditions. For that reason we pay special attention to these cases in the last part of this Section.

We have also focused on the behavior of the asymptotic coarse-grained current as a function of the width in p of the initial mixed superposition of momentum eigenstates

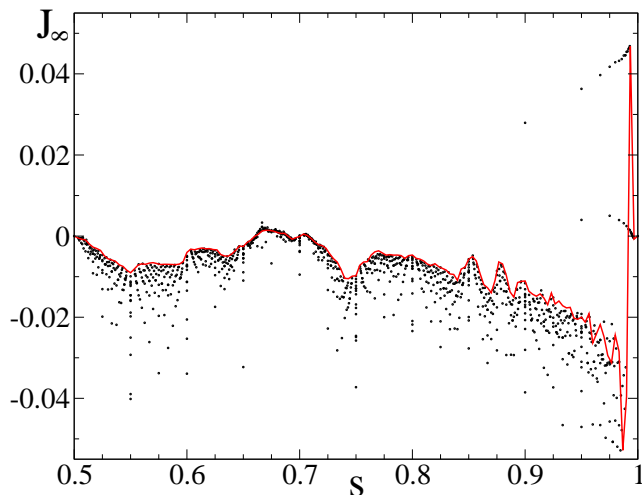


Figure 2: (Color online) Asymptotic coarse-grained current J_∞ for the AQMBM as a function of $s = D_1/D$, for all possible values of $D_1 \geq D/2$. The asymptotic current is represented by a solid line for $D = 300$ and with dots for lower values. The initial state is an equal probability mixture of $\Delta p = D/10$ central momentum eigenstates of the cell.

The values of J_∞ for a fixed dimension $D = 100$, different Δp and as a function of s , can be seen in Fig. 3. The current decreases with the width of the momentum band in the region of $s \lesssim 0.7$. Nevertheless, for $s \gtrsim 0.7$ we can see that by enlarging the width of the initial distribution up to approximately a 60% of the maximum phase space size in momentum, the fluctuations become smoother. However, it is remarkable that the current nearly vanishes in the same region where the convergence to the classical behavior is faster. For greater Δp values the current decreases strongly, and for a distribution over all the p range there is no current.

Finally, in view of the relevance that the operator $\hat{B}_{s,k}$ has in the properties of J_∞ , we have studied some features of its spectrum for different values of s . We display the eigenphases θ (in units of π) as a function of k in Fig. 4, for $D = 30$. The spectrum for the case $D_1 = 15$, for which the symmetry S_I is present, is invariant under reflections at $k = \pi$. This is due to the fact that $\hat{B}_{s,k}$ is invariant under $k \rightarrow 2\pi - k$, up to an even number of row permutations. The periodicity in k makes the spectrum symmetric with respect to $k = 0$ also. This symmetry is absent for all the other values of s . We have considered the less asymmetric case $D_1 = 16$, and an intermediate one with $D_1 = 26$, where this becomes already evident. Finally, for $D_1 = 29$ we can see a very regular spectrum, similar to those of integrable systems, that nevertheless shows level repulsion. In all cases, there is a symmetry given by the transformation $k \rightarrow k + \pi$, $\theta \rightarrow \theta + \pi$ since $\hat{B}_{s,k+\pi} = -\hat{B}_{s,k}$, and therefore any eigenstate of $\hat{B}_{s,k+\pi}$ ($|\phi_l(k + \pi)\rangle$) will be also an eigenstate of $\hat{B}_{s,k}$ with eigenvalue $\theta_{kl} = \theta_{k+\pi l} + \pi$.

We have analyzed the cumulative level spacing distri-

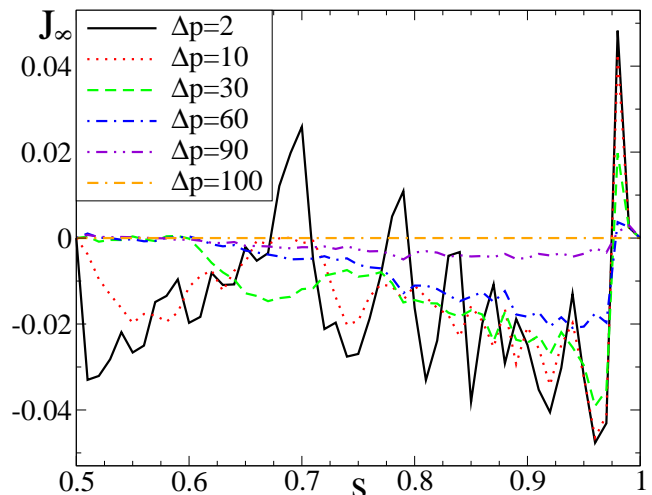


Figure 3: (Color online) Asymptotic coarse-grained current J_∞ for the AQMBM as a function of $s = D_1/D$ and for a fixed $D = 100$. The initial states and values of s are taken as in Fig. 2, but for Δp equal to 2, 10, 30, 60, 90 and 100.

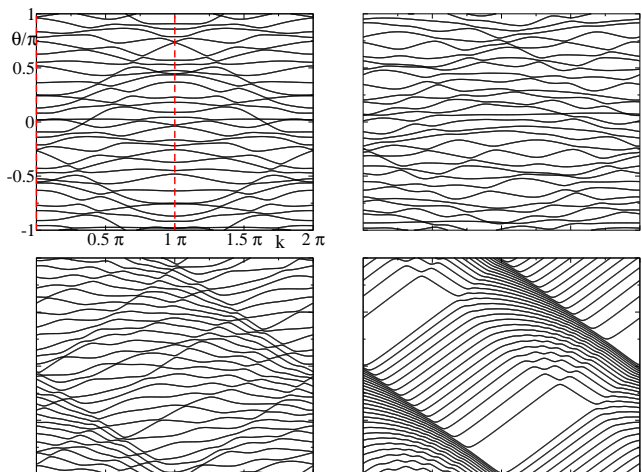


Figure 4: Eigenphases θ (in units of π) of the AQMBM as a function of k for $D = 30$. On the top panels we can find them for $D_1 = 15$ (left) and $D_1 = 16$ (right), and on the bottom ones for $D_1 = 26$ (left) and $D_1 = 29$ (right). For $D_1 = 15 = D/2$, the spectrum has a reflection symmetry at $k = \pi$ and $k = 0$ (both indicated with red dashed lines).

bution of the AQMBM averaged in k ,

$$I(\theta) = \int dk/(2\pi) \int_0^\theta d\theta' P(\theta'), \quad (27)$$

where $P(\theta)$ corresponds to the level spacing distribution. The results are shown in Fig. 5. We have taken the phase θ normalized by the mean level spacing $2\pi/D$. It becomes clear that the behavior of the case of the last panel in Fig. 4 ($D_1 = 29$) is completely different from the rest, confirming our previous conclusions. In fact,

it is very close to the Poisson distribution, which corresponds to integrable or regular systems. Level repulsion is also evident since for small θ values, the curve corresponding to the AQMBM levels shows its main difference with respect to the Poisson one. The other cases are very close to the Wigner–Dyson shape (CUE), that corresponds to the typical behavior of chaotic systems. It has to be underlined the very good agreement we have found for the symmetrical case. We can conclude that the quasi-regular behavior of the most asymmetric cases, i.e. the one we show for $D_1 = 29$ and the one for $D_1 = 28$ which is very similar to it, is highly anomalous. This is in close relation to the exceptional current values found for $D_1 = D - 1$ and $D_1 = D - 2$ in Fig. 2.

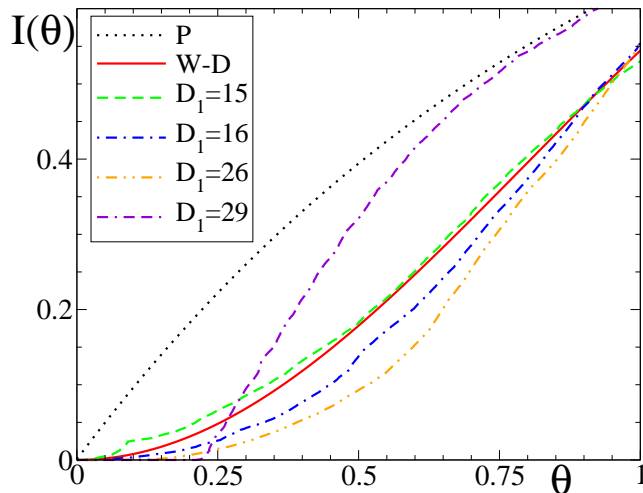


Figure 5: (Color online) Cumulative level spacing $I(\theta)$ of the AQMBM averaged in k (θ is in units of the mean level spacing $2\pi/D$). This is shown for the Poisson and Wigner–Dyson distributions and for the AQMBMs displayed on Fig. 4 ($D = 30$; $D_1 = 15$, $D_1 = 16$, $D_1 = 26$ and $D_1 = 29$). See inset for references.

IV. CURRENT GENERATION

In order to understand the origin of the directed current we have analyzed the classical and quantum phase space distributions for given initial conditions, as a function of time. We have studied them for short times and a Hilbert space dimension $D \leq 80$, which is of the order of the Hilbert space dimensions of the cells we have used in obtaining the results of Section III. The choice of these evolution times and dimensions is suitable since it makes the phase space representations more clear and the departure of the quantum distributions from the classical behavior is already present. In fact, for our system this time can be extremely short, as we will see in the following. Then, although the asymptotic limit of the current J_∞ is still far from being reached, the mechanisms that give rise to the current can be seen.

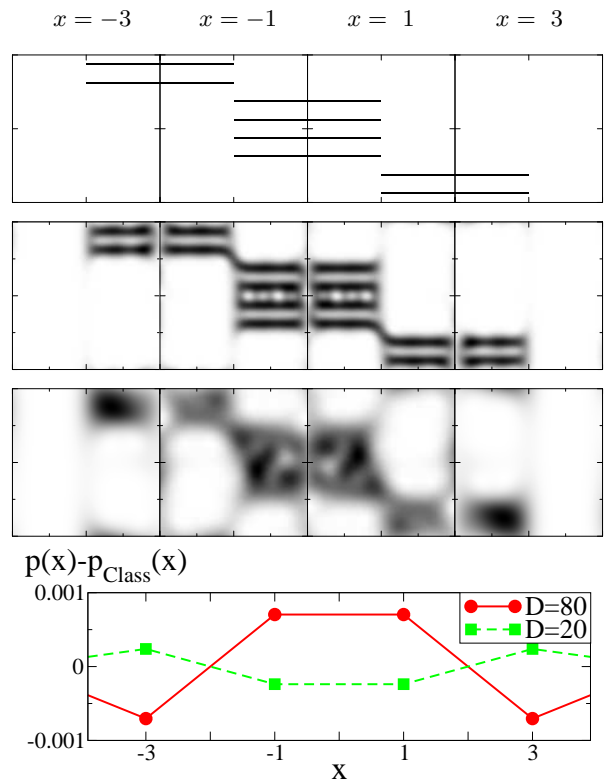


Figure 6: (Color online) In the top panel we show the phase space of the classical Multibaker map with $s = 0.5$ for a momentum centered strip of width $\delta p = 0.1$ evolved 3 times. Only the sites with $x = -3, -1, 1, 3$ are shown. In the middle top and bottom panels the Husimi function is shown for the quantum version of the map ($D = 80$ and $D = 20$, respectively). Finally, in the bottom panel we show the difference $p(x, t) - p_{class}(x, t)$ (see main text for details).

An initial distribution corresponding to a momentum centered strip of width $\delta p = 0.1$ and its quantum analogues have been evolved up to three time steps of the map. Results for $s = 0.5$ are displayed in Fig. 6, while the ones for $s = 0.75$ are shown in Fig. 7. In the top panels of both Figures we can see the classical distribution corresponding to the cells at lattice positions $x = -3, -1, 1, 3$, given that for $x = -2, 0, 2$ they are empty (this is a result of the translation operator and the initial conditions choice). In the middle ($D = 80$) and bottom ($D = 20$) panels we show the corresponding Husimi distributions, taking quantum initial conditions in the same way as in Section III. Finally, in the bottom panels we can find the probability distribution difference given by $p(x, t) - p_{class}(x, t)$.

By comparing both Figures we can immediately notice that the classical distribution $p_{class}(x, t)$ for $s = 0.5$ keeps its initial symmetry. The quantum distributions in both cases considered also keep it. But for $s = 0.75$ the situation changes. Now, the classical probability is not symmetrical but it is still balanced with respect to the origin (a given distribution is balanced if $\langle x \rangle = 0$).

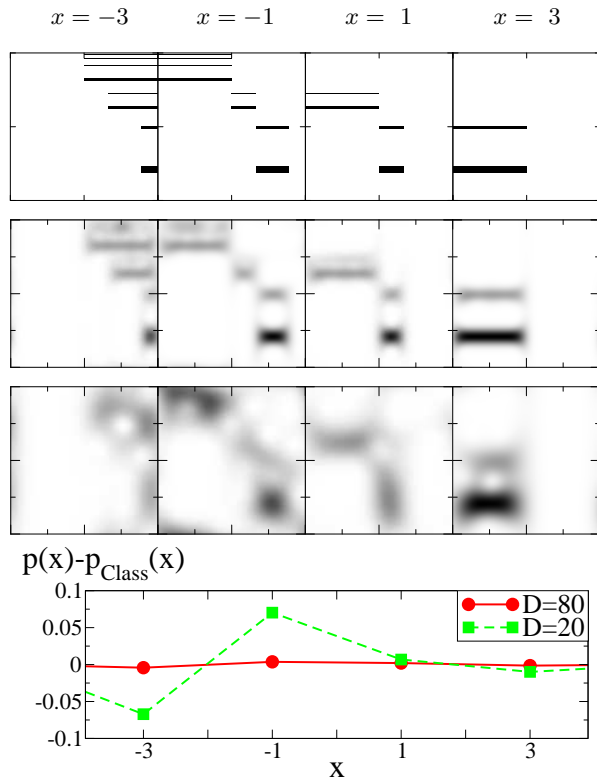


Figure 7: (Color online) In the top panel we show the phase space of the classical Multibaker map with $s = 0.75$ for a momentum centered strip of width $\delta p = 0.1$ evolved 3 times. Only the sites with $x = -3, -1, 1, 3$ are shown. In the middle top and bottom panels the Husimi function is shown for the quantum version of the map ($D = 80$ and $D = 20$, respectively). Finally, in the bottom panel we show the difference $p(x, t) - p_{class}(x, t)$ (see main text for details).

This asymmetry is also present in the quantum case, but the balance of the distribution is broken due to interference effects. In fact, if we look at the lower panel of Fig. 6 we can see that the quantum and classical distributions have almost equal weights in each cell (apart from quantum fluctuations). But the lower panel of Fig. 7 clearly shows that for the $D = 20$ case, the imbalance in the $p(x, t)$ distribution is already present. For $D = 80$ we still have a close quantum-classical correspondence for this short evolution time. This fact underlines the fundamental role that quantum effects play in the net current appearance. It is clear that at times of the order of the Ehrenfest time ($t \sim \log_2 D$) the imbalance starts to build up. This imbalance evolves in time shaping the $p(x, t)$ distribution. At the order of the Heisenberg time (which in this case corresponds to $t \sim D$) the asymptotic current is reached. We show the shape of $p_{class}(x, t)$ and $p(x, t)$ for the cases $D = 20$ and $D = 80$ in Fig. 8, where we have taken $s = 0.75$ and $t = 80$. This illustrates how

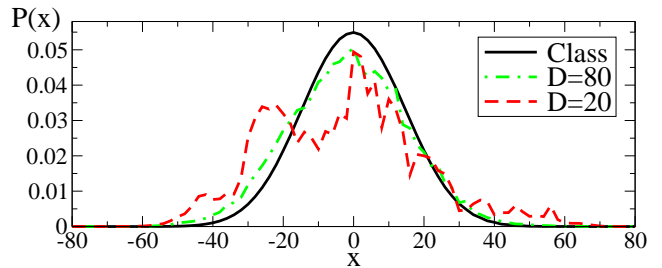


Figure 8: (Color online) Classical $p_{class}(x, t)$ (solid black line) and quantum $p(x, t)$ (dot-dashed green line for $D = 80$ and dashed red line for $D = 20$) distributions, taking $s = 0.75$ and $t = 80$.

V. CONCLUSIONS

In this work we have studied a recently introduced model for purely quantum directed transport, which shows a finite asymptotic current. We have analyzed the way in which the net transport appears by studying the classical and quantum phase space distributions for short times, showing the results for $t = 3$. In the symmetric case $s = 0.5$, the classical and quantum distributions retain the symmetry around $x = 0$ and therefore both currents are forbidden. In the $s \neq 0$ case both distributions are asymmetric. The classical one is always balanced ($\langle x \rangle = 0$), while the quantum one develops imbalances leading to the appearance of a net current. This is clearly a purely quantum effect due to interferences.

We have also studied several features of this phenomenon, in particular the dependence on the asymmetry parameter and the value of h . We could notice a marked dependence of the J_∞ behavior on the values of s . In fact we observe a faster vanishing of the transport for $s < 0.7$ both as $h \rightarrow 0$ and as the width of the initial conditions $\delta p \rightarrow 1$. We have found that for the higher values of s the spectrum behavior approaches that of an integrable system (nevertheless with notable discrepancies, specially for small level spacings since no degeneracies are present).

We would like to mention that the mechanisms behind the current generation in our system are different from previously studied quantum ratchet accelerators [11, 15], where there is a ballistic energy growth. Here, there is no need to control this effect since the asymptotic current is finite.

Acknowledgments

Partial support by ANPCyT and CONICET is gratefully acknowledged.

-
- [1] R. P. Feynman, *Lectures on Physics*, **Vol. 1**, (Addison-Wesley, Reading, MA, 1963).
- [2] S. Flach *et al.*, Phys. Rev. Lett. **84**, 2358 (2000); S. Denisov and S. Flach, Phys. Rev. E **64**, 056236 (2001); S. Denisov *et al.*, Physica D **170**, 131 (2002).
- [3] P. Jung *et al.*, Phys. Rev. Lett. **76**, 3436 (1996); J.L. Mateos, Phys. Rev. Lett. **84**, 258 (2000).
- [4] H. Schanz *et al.*, Phys. Rev. Lett. **87**, 070601 (2001); S. Denisov *et al.*, Phys. Rev. E **66**, 046203 (2002); H. Schanz *et al.*, Phys. Rev. E **71**, 026228 (2005).
- [5] S. Denisov, L. Morales-Molina, S. Flach, and P. Hänggi, Phys. Rev. A **75**, 063424 (2007).
- [6] P. Reimann *et al.*, Phys. Rev. Lett. **79**, 10 (1997); I. Franco and P. Brumer, Phys. Rev. Lett. **97**, 040402 (2006).
- [7] P. Reimann, Phys. Rep. **361**, 57 (2002).
- [8] F. Jülicher *et al.*, Rev. Mod. Phys. **69**, 1269 (1997).
- [9] R.D. Astumian, Science **276**, 917 (1997).
- [10] C. Mennerat-Robilliard *et al.*, Phys. Rev. Lett. **82**, 851 (1999). P.H. Jones *et al.*, Phys. Rev. Lett. **98** 073002 (2007).
- [11] M. Sadgrove, M. Horikoshi, T. Sekimura, and K. Nakagawa, Phys. Rev. Lett. **99**, 043002 (2007); I. Dana, V. Ramareddy, I. Talukdar, and G.S. Summy, Phys. Rev. Lett. **100**, 024103 (2008).
- [12] F.L. Moore *et al.*, Phys. Rev. Lett. **75**, 4598 (1995); T.S. Monteiro *et al.*, Phys. Rev. Lett. **89**, 194102 (2002); G.G. Carlo *et al.* Phys. Rev. Lett. **94**, 164101 (2005); G.G. Carlo *et al.* Phys. Rev. A **74**, 033617 (2006).
- [13] E. Lundh and M. Wallin, Phys. Rev. Lett. **94**, 110603 (2005); E. Lundh, Phys. Rev. E **74** 016212 (2006); D. Poletti *et al.*, Phys. Rev. E **75**, 011102 (2007).
- [14] A. Kenfack, J. Gong, and A.K. Pattanayak, Phys. Rev. Lett. **100**, 044104 (2008); J. Wang and J. Gong, arXiv:0806.3842.
- [15] M. Sadgrove, M. Horikoshi, T. Sekimura, and K. Nakagawa, Eur. Phys. J. D **45**, 229 (2007)
- [16] L. Ermann, G.G. Carlo, and M. Saraceno, Phys. Rev. E **77**, 011126 (2008).
- [17] P. Gaspard, J. Stat. Phys. **68** (5/6) 673 (1992); S. Tasaki and P. Gaspard, J. Stat. Phys. **81**, (5/6) 935-987 (1995).
- [18] D.K. Wójcik and J.R. Dorfman, Phys. Rev. E **66**, 036110 (2002); D.K. Wójcik and J.R. Dorfman, Phys. Rev. Lett. **90**, 230602 (2003); D.K. Wójcik and J.R. Dorfman, Physica D **187**, 223 (2004); D.K. Wójcik Int. J. Mod. Phys. B **20**, 1969 (2006).
- [19] L. Ermann, J.P. Paz, and M. Saraceno, Phys. Rev. A **73**, 012302 (2006).
- [20] N.L. Balazs and A. Voros, Ann. Phys. **190**, 1 (1989).
- [21] M. Saraceno, Ann. Phys. **199**, 37 (1990).
- [22] T.A. Brun, H.A. Carteret and A. Ambainis, Phys. Rev. A **67**, 052317 (2003).